The International Journal of Biochemistry & Cell Biology 64 (2015) 15–24

Contents lists available at ScienceDirect

The International Journal of Biochemistry & Cell Biology

journal homepage: www.elsevier.com/locate/biocel

Functional and structural interaction of (−)-lobeline with human α4β2 and α4β4 nicotinic acetylcholine receptor subtypes

Hugo R. Arias [a,*], Dominik Feuerbach [b], Marcelo Ortells [c]

[a] Department of Medical Education, California Northstate University College of Medicine, Elk Grove, CA, USA
[b] Neuroscience Research, Novartis Institutes for Biomedical Research, Basel, Switzerland
[c] Faculty of Medicine and CONICET, University of Morón, Argentina

ARTICLE INFO

Article history:
Received 9 January 2015
Received in revised form 2 March 2015
Accepted 9 March 2015
Available online 18 March 2015

Keywords:
Human α4β2 and α4β4 nicotinic acetylcholine receptors
(−)-Lobeline
Competitive antagonist
Ca^{2+} influx
Molecular modeling

ABSTRACT

To determine the pharmacologic activity of (−)-lobeline between human (h)α4β2 and hα4β4 nicotinic acetylcholine receptors (AChRs), functional and structural experiments were performed. The Ca^{2+} influx results established that (−)-lobeline neither actives nor enhances the function of the studied AChR subtypes, but competitively inhibits hα4β4 AChRs with potency ~10-fold higher than that for hα4β2 AChRs. This difference is due to a higher binding affinity for the [^{3}H]cytisine sites at hα4β4 compared to hα4β2 AChRs, which, in turn, can be explained by our molecular dynamics (MD) results: (1) higher stability of (−)-lobeline and its hydrogen bonds within the α4β4 pocket compared to the α4β2 pocket, (2) (−)-lobeline promotes Loop C to cap the binding site at the α4β4 pocket, but forces Loop C to get apart from the α4β2 pocket, precluding the gating process elicited by agonists, and (3) the orientation of (−)-lobeline within the α4β4, but not the α4β2, subpocket, promoted by the *t*− (or *t*+) rotameric state of α4-Tyr98, remains unchanged during the whole MD simulation. This study gives a detailed view of the molecular and dynamics events evoked by (−)-lobeline supporting the differential binding affinity and subsequent inhibitory potency between hα4β2 and hα4β4 AChRs, and supports the possibility that the latter subtype is also involved in its activity.

1. Introduction

(−)-Lobeline [(−)-2S, 6R, 8S-lobeline, or α-lobeline] is a non-pyridino alkaloid obtained from several *Lobelia* plant species. Pre-clinical and clinical studies have demonstrated that this natural product possess pro-cognitive activity in animals (Decker et al., 1993) and in patients with attention deficit hyperactivity disorder (Martin et al., 2015), as well as anxiolytic (Brioni et al., 1993), and anti-addictive (Harrod et al., 2001; Polston et al., 2006) properties. Although (−)-lobeline was used as a smoking cessation agent, several side effects made this drug to be banned by the FDA (reviewed in Sewester et al., 1997).

Although (−)-lobeline was originally classified as a partial agonist of nicotinic acetylcholine receptors (AChRs), mounting evidence suggests that this compound behaves more like a competitive antagonist. Although (−)-lobeline binds to AChRs with high affinity (K_i ~4 nM) (Flammia et al., 1999), the functional results indicate that it does not activate (Damaj et al., 1997) or slightly activates (Kaniaková et al., 2011) AChRs, but instead it acts as an antagonist at different AChRs (Dwoskin and Crooks, 2002). It has been hypothesized that the previously described pharmacologic activities of (−)-lobeline are mediated by its interaction with α4β2 AChRs. However, the evidence indicating that (−)-lobeline-induced [^{3}H]dopamine overflow from rat striatal slices is not inhibited by mecamylamine (Dwoskin and Crooks, 2002), a nonspecific noncompetitive antagonist of AChRs, and that the spinal analgesic activity of (−)-lobeline does not correlate with its affinity at the α4β2 AChR (Flammia et al., 1999), suggests additional mechanisms of action (Dwoskin and Crooks, 2002; Kaniaková et al., 2011) or the existence of other targets. For example, it has been suggested that (−)-lobeline may interact with a locus different from the

Abbreviations: AChR, nicotinic acetylcholine receptor; (−)-lobeline (α-lobeline) (−), -2S, 6R, 8S-lobeline, Ct-AChBP, acetylcholine binding protein from *Capitella teleta*; Ac-AChBP, acetylcholine binding protein from *Aplysia californica*; CCh, carbamylcholine; RT, room temperature; BS, binding saline; EXD, extracellular domain, ORT, orthosteric; K_i, inhibition constant; K_d, dissociation constant; IC_{50}, ligand concentration that produces 50% inhibition (of binding or of agonist activation); n_H, Hill coefficient; EC_{50}, agonist concentration that produces 50% AChR activation; MD, molecular dynamics; FBS, fetal bovine serum.

* Corresponding author at: Department of Medical Education, California Northstate University College of Medicine, 9700 W. Taron Dr., Elk Grove, CA 95757, USA. Tel.: +1 916 647 0458; fax: +1 916 686 7310.
E-mail address: hugo.arias@cnsu.edu (H.R. Arias).

http://dx.doi.org/10.1016/j.biocel.2015.03.003
1357-2725/

orthosteric sites enhancing agonist-activated α4β2 AChRs (Kaniaková et al., 2011), a pharmacologic property resembling that for positive allosteric modulators (reviewed in Arias, 2011).

There is a large amount of experimental evidence supporting an important role of α4β2 AChRs in the mechanism of nicotine addiction (reviewed in Ortells and Arias, 2010). For example, knockout animal results indicate that the β2 subunit is necessary for nicotine-induced dopamine release (Grady et al., 2001), and for the discriminative (Shoaib et al., 2002) and reinforcing (Picciotto et al., 1998) properties of nicotine. Although α4β4 AChRs are expressed in less proportion compared to α4β2 AChRs, they have been found in several brain regions, including basal ganglia, cerebellum, midbrain, ventral tegmental area, hippocampus, and cortex, where some of these areas are implicated in drug addiction (Azam et al., 2002; Quik et al., 2000).

Studies using the acetylcholine binding proteins (AChBPs) from *Capitella teleta* (Ct-AChBP; Billen et al., 2012), and *Aplysia californica* (Ac-AChBP; Hansen et al., 2005) show that (−)-lobeline induces a strong capping of Loop C (at the principal component) as other antagonists do, as well as exposes an additional subpocket to accommodate the α-hydroxyphenetyl moiety by changing the rotameric state of a Tyr residue from Loop A, the so-called g-to-t or Tyr-flip conformation (reviewed in Arias, 2012). Since (−)-lobeline presents interesting pharmacologic properties and could be clinically important, the binding affinity, agonistic and antagonistic activities of (−)-lobeline, as well as the structural features of its binding site were compared between the human (h) α4β2 and hα4β4 AChRs. In this regard, Ca^{2+} influx and [^{3}H]cytisine competition binding assays, as well as molecular docking and molecular dynamics (MD) studies were applied.

2. Materials and methods

2.1. Materials

[^{3}H]Cytisine (40 Ci/mmol) was obtained from PerkinElmer Life Sciences Products, Inc. (Boston, MA, USA), and stored at −20 °C. Carbamylcholine dihydrochloride (CCh), (−)-lobeline hydrochloride and polyethylenimine were purchased from Sigma Chemical Co. (St. Louis, MO, USA), whereas probenecid was obtained from Sigma Chemical Co. (Buchs, Switzerland). (±)-Epibatidine hydrochloride was obtained from Tocris Bioscience (Ellisville, MO, USA). Fluo-4 was purchased from Molecular Probes (Eugene, OR, USA). Fetal bovine serum (FBS) and trypsin/EDTA were purchased form Gibco BRL (Paisley, UK). Salts were of analytical grade.

2.2. Ca^{2+} influx measurements in HEK293-hα4β2 and CHO-hα4β4 cells

Ca^{2+} influx assays were performed as previously described (Pérez et al., 2013; Arias et al., 2013, 2015). Briefly, HEK293-hα4β2 and CHO-hα4β4 cells were seeded 72 h prior to the experiment on black 96-well plates (Costar, New York, USA) at a density of 5×10^4 per well and incubated at 37 °C in a humidified atmosphere (5% CO_2/95% air). 16–24 h before the experiment, the medium was changed to 1% FBS in HEPES-buffered salt solution (HBSS) (130 mM NaCl, 5.4 mM KCl, 2 mM $CaCl_2$, 0.8 mM $MgSO_4$, 0.9 mM NaH_2PO_4, 25 mM glucose, 20 mM HEPES, pH 7.4). On the day of the experiment, the medium was removed by flicking the plates and replaced with 100 μL HBSS/1% FBS containing 2 μM Fluo-4 in the presence of 2.5 mM probenecid. The cells were then incubated at 37 °C in a humidified atmosphere (5% CO_2/95% air) for 1 h. Plates were flicked to remove excess of Fluo-4, washed twice with HBSS/1% FBS, and finally refilled with 100 μL of HBSS containing different concentrations of (−)-lobeline and pre-incubated for 5 min. Plates were then placed in the cell plate stage of the fluorimetric imaging plate reader (FLIPR; Molecular Devices, Sunnyvale, CA, USA). (±)-Epibatidine (0.1 μM) was then added from the agonist plate to the cell plate using the 96-tip pipettor simultaneously to fluorescence recordings for a total length of 3 min. A baseline consisting of 5 measurements of 0.4 s each was recorded. To determine the agonistic activity, AChRs were stimulated with increasing concentrations of (−)-lobeline. In parallel experiments, a fixed concentration of (±)-epibatidine (i.e., 1, 3, 10, 30, or 100 nM) was co-injected with increasing concentrations of (−)-lobeline. The excitation and emission wavelengths are 488 and 510 nm, at 1 W, and a CCD camera opening of 0.4 s.

2.3. [^{3}H]Cytisine competition binding experiments

To determine the binding affinity of (−)-lobeline for the hα4β2 and hα4β4 AChRs, [^{3}H]cytisine competition binding experiments were performed as previously published (Pérez et al., 2013; Arias et al., 2015). In this regard, AChR membranes (1.0 mg/mL), first prepared from HEK293-hα4β2 and CHO-hα4β4 cells (Pérez et al., 2013; Arias et al., 2015), were suspended in BS buffer with 10 nM [^{3}H]cytisine, and preincubated for ~30 min at RT. Nonspecific binding was determined in the presence of 1 mM CCh. The total volume was divided into aliquots, and increasing concentrations of (−)-lobeline were added to each tube and incubated for 2 h at RT. AChR-bound [^{3}H]cytisine was then separated from free radioligand by a filtration assay using a 48-sample harvester system with GF/B Whatman filters (Brandel Inc., Gaithersburg, MD, USA), previously soaked with 0.5% polyethylenimine for 30 min. The membrane-containing filters were transferred to scintillation vials with 3 mL of Bio-Safe II (Research Product International Corp, Mount Prospect, IL, USA), and the radioactivity was determined using a Beckman LS6500 scintillation counter (Beckman Coulter, Inc., Fullerton, CA, USA).

The concentration–response data were curve-fitted by nonlinear least squares analysis using the Prism software (GraphPad Software, San Diego, CA). The observed IC_{50} values were transformed into inhibition constant (K_i) values using the Cheng–Prusoff relationship (Cheng and Prusoff, 1973):

$$K_i = \frac{IC_{50}}{1 + ([[^3H]\text{cytisine}]/K_d^{\text{cytisine}})} \quad (1)$$

where [[^{3}H]cytisine] is the initial concentration of [^{3}H]cytisine, and K_d^{cytisine} is the dissociation constant for [^{3}H]cytisine at the hα4β4 (0.1 nM; Slater et al., 2003) and hα4β2 AChRs (0.3 nM; Zhang and Steinbach, 2003), respectively. The calculated K_i values were summarized in Table 1.

2.4. Homology models of the α4β4 and α4β2 subunit pairs

Structural models of the α4β2 and α4β4 subunit pairs were based on the crystal structure of the Ct-AChBP complexed with (−)-lobeline (PDB 4AFH; Billen et al., 2012) as a template for

Table 1
Inhibitory potency (IC_{50}) and binding affinity (K_i) of (−)-lobeline for the hα4β2 and hα4β4 AChRs.

AChR subtype	Ca^{2+} influx		[^{3}H]Cytisine competition binding	
	IC_{50} [a] (μM)	n_H [a]	K_i [b] (nM)	n_H [b]
hα4β4	0.25 ± 0.04	1.67 ± 0.17	1.82 ± 0.07	0.87 ± 0.03
hα4β2	2.58 ± 0.50	1.06 ± 0.11	4.90 ± 0.30	0.79 ± 0.04

n_H, Hill coefficient.
[a] These values were obtained from Fig. 1A and C, respectively.
[b] These values were obtained from experiments as shown in Fig. 2.

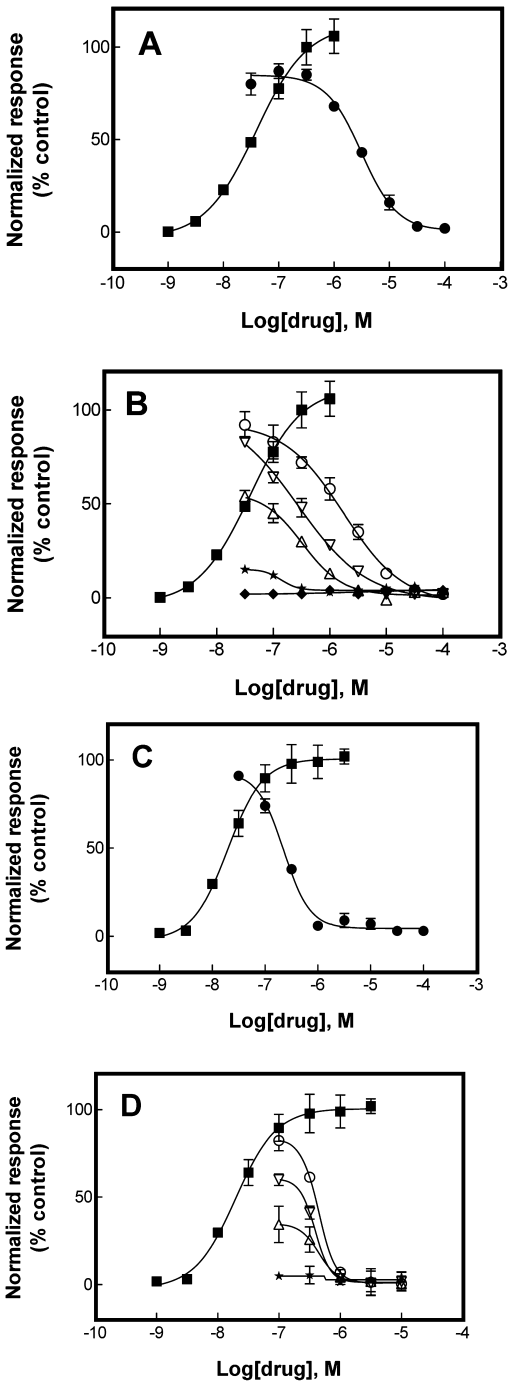

Fig. 1. (−)-Lobeline induced inhibition of (±)-epibatidine-evoked calcium influx in HEK293-hα4β2 and CHO-hα4β4 cells. Increased concentrations of (±)-epibatidine (■) activate the hα4β2 (EC_{50} = 30 ± 5 nM; n_H = 1.03 ± 0.04; n = 21) (A and B) and hα4β4 (EC_{50} = 9.6 ± 2.0 nM; n_H = 1.01 ± 0.03; n = 18) (C and D) AChRs with different potency. (A and C) To determine the antagonistic activity of (−)-lobeline, cells were pre-treated with several concentrations of (−)-lobeline (●) followed by addition of 0.1 μM (±)-epibatidine. (B and D) Co-injection of (±)-epibatidine [i.e., (♦) 1, (★) 3, (△) 10, (▽) 30, or (○) 100 nM] and increasing concentrations of (−)-lobeline at each cell line. Representative graphs for (−)-lobeline are based on six (A), four (C), and three (B and D) experiments, respectively. The error bars represent the standard deviation (SD). Ligand response was normalized to the maximal (±)-epibatidine response, which was set as 100%. The calculated IC_{50} and n_H values are summarized in Table 1.

the AChR extracellular domain (EXD). The α4β2- and α4β4-EXD models were built by homology modeling using Modeller 9.8 (Šali and Blundell, 1993) and SWIFT MODELLER (Mathur and Shankaracharya Vidyarthi, 2011). For this purposes, the amino acid sequences of the studied AChR subunits (i.e., hα4, hβ2, and hβ4)

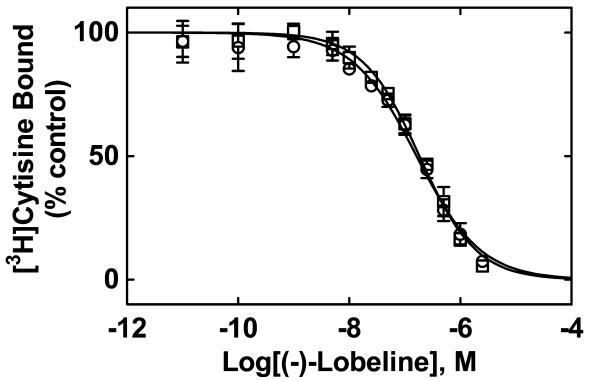

Fig. 2. (−)-Lobeline-induced inhibition of [^{3}H]cytisine binding to hα4β4 (□) and hα4β2 (○) AChRs, respectively. AChR membranes (1.0 mg/mL) were pre-incubated (30 min) with 10 nM [^{3}H]cytisine, and then equilibrated (2 h) with increasing concentrations of (−)-lobeline. Nonspecific binding was determined at 1 mM CCh. Each plot was performed in triplicate, and the error bars correspond to the SD. At least two separated experiments were combined and the IC_{50} and n_H values obtained by linear regression. Subsequently, the K_i values were calculated according to Eq. (1). The K_i and n_H values were summarized in Table 1.

were aligned with the sequences of Ct-AChBP and Ac-AChBP by using the ClustalW2 server (www.ebi.ac.uk/Tools/msa/clustalw2) (Thompson et al., 1994).

The binding site models were constructed using two neighboring subunits of the five subunits from the original template containing the agonist binding site domain. Since Ct-AChBP is complexed with (−)-lobeline in the five subunits and no binding differences were observed by the authors (Billen et al., 2012), any subunit pair can be used to delineate the α4/β2 and α4/β4 binding site interfaces. The use of only two subunits, those that conform the binding site, instead of modeling the whole extracellular pentamer, is justified by the fact that no cooperative interaction between (−)-lobeline and each AChR subtype is observed (see [^{3}H]cytisine competitive binding results in Fig. 2), indicating binding equivalence between both binding sites from each AChR subtype.

The subunit combinations α4(+)/β2(−) and α4(+)/β4(−) were modeled without (i.e., Apo form) and with (−)-lobeline (i.e., bound form). (−)-Lobeline and water molecules were added to the model according to the AChBP-lobeline structure (Billen et al., 2012). The models were energy minimized using molecular mechanics (Keserü and Kolossváry, 1999) and the software NAMD (CVS-2013-07-06 for Linux x86, 64bits multicore CUDA version; Phillips et al., 2005), CHARMM force field (Brooks et al., 1983), and VEGA ZZ (Pedretti et al., 2004). To avoid distorting the protein secondary structure, the energy minimization was carried out fixing the backbone atoms to their original positions. The systems were fully minimized using NAMD. These minimized conformations changed during the course of the MD simulations as expected.

2.5. Molecular dynamics simulations

To determine any conformational change on Loop C when (−)-lobeline binds to each site, a series of MD simulations of the orthosteric binding sites, including the whole Loop C, were performed using the α4β2 and α4β4 subunit interfaces, without (i.e., Apo form) and with (−)-lobeline (i.e., bound form). To reduce computing time, only protein residues and water molecules within a 40 Å sphere centered on the Cys–Cys pair found in Loop C and the Loop C itself, were allowed to move freely. To restrict the MD simulations to a defined space, spherical periodic boundary conditions (Lewards, 2011) were implemented with center at the center of mass at each subunit pair. The MD simulations spanning 20-ns were performed using NAMD and CHARMM force field. The

protocol included a timestep size of 1 fs, with 20 timesteps per cycle (the number of timesteps between atom reassignments). The cutoff value for non-bond energy evaluation was 12 Å. A distance of 8 Å for the switching function was used. Pairs of bonded atoms excluded from non-bonded interaction calculations was determined to 1–4, that is, no non-bonded interactions were calculated for lists of 4 consecutive bonded atoms. The temperature of the system was rescaled every 1000 steps to 300 K. To determine the stability of Loop C and (−)-lobeline, the root mean square deviation (RMSD) values extracted from the MD for the α4β2 and α4β4 subunit pairs was calculated using VEGA ZZ (Pedretti et al., 2004). The RMSD values, representing the inter-molecular conformational changes and the translation of the whole molecule in the binding site, were calculated using the following equation:

$$\mathrm{RMSD} = \sqrt{\frac{\sum_{i=1}^{N} \partial_i^2}{N}} \quad (2)$$

where N is the number of atoms from the ligand, and ∂_i^2 is the distance between the corresponding ligand atoms obtained at each step and the starting conformation.

To study the interaction of (−)-lobeline with its subpocket, the conformational changes of the α4-Tyr98 side chain elicited by (−)-lobeline during the 20-ns MD simulations were determined. α4-Tyr98 is the homologous of the Tyr residue observed in AChBPs having an unusual rotameric t-state (reviewed in Arias, 2012). The chi1 values obtained from the simulations were used for the analysis of the rotameric states at both (−)-lobeline-AChRs complexes.

To measure the occurrence of hydrogen bonding for (−)-lobeline at each dimer during the MD simulations as well as the occupancy of every hydrogen bond (i.e., the percentage of the MD where a hydrogen bond is present), the H-bond plugin version 1.2 of the VMD program version 1.9.1 (Humphrey et al., 1996) was used. To obtain a clearer view of the hydrogen bonding patterns, the mobile means of hydrogen bonds during the MDs was calculated as the average number of hydrogen bonds present in temporal windows of 100 fs.

To estimate the binding energies for (−)-lobeline at the α4β4 and α4β2 subunit pairs, potential energies from the ligand-receptor complexes, and from the isolated α4β4 and α4β2 subunit pairs and isolated ligand were calculated using molecular mechanics (Keserü and Kolossváry, 1999), for the initial (minimized) state and for the last 10-ns of the simulations. For the isolated (−)-lobeline, the ligand structure solved in the (−)-lobeline-Ct-AChBP complex was extracted and minimized alone. For the last 10-ns of the simulations, mean energies were used, i.e. the energy averages estimated during the last 10,000 steps (1 step, 1 fs) of each MD.

3. Results

3.1. Pharmacologic activity of (−)-lobeline at the HEK293-hα4β2 and CHO-hα4β4 cells assessed by Ca^{2+} Influx

The pharmacologic activity of (−)-lobeline was compared to that for (±)-epibatidine by assessing the fluorescence change on each AChR-expressing cell line (Fig. 1). The results indicate that (−)-lobeline stimulates neither AChR subtype, whereas (±)-epibatidine activates them with the following potency: $EC_{50} = 30 \pm 5$ nM (hα4β2) (Fig. 1A) and 9.6 ± 2.0 nM (hα4β4) (Fig. 1C). This indicates that hα4β4 AChRs are 3-fold more sensitive than hα4β2 AChRs to the agonistic activity of (±)-epibatidine. The results on hα4β2 AChRs correspond very well with previous data (Pérez et al., 2013), whereas the results on hα4β4 AChRs are lower than previous estimations (~38 nM) (Stauderman et al., 1998). The calculated n_H values: 1.03 ± 0.04 for the hα4β2 (Fig. 1A) and 1.01 ± 0.03 for the hα4β2 (Fig. 1C), indicate that (±)-epibatidine activates the AChRs by a non-cooperative mechanism, suggesting that the agonist cannot distinguish between both binding sites.

The antagonistic properties of (−)-lobeline were also investigated by pre-incubating the AChR with (−)-lobeline before the (±)-epibatidine-induced AChR activation (Fig. 1A and C). In this regard, (−)-lobeline inactivates the hα4β4 AChR with potency ($IC_{50} = 0.25 \pm 0.04$ μM) ~10-fold higher than that for the hα4β2 (2.58 ± 0.50 μM) (Table 1). The observed n_H value for the hα4β2 AChR is close to unity (Table 1), suggesting that the ligand inhibits this receptor by a non-cooperative mechanism, whereas the value for the hα4β4 AChR is higher than unity, suggesting a cooperative mechanism. The cooperative behavior, in turn, suggests that (−)-lobeline may discriminate between both agonist binding sites at the hα4β4 AChR.

To determine whether (−)-lobeline potentiates the activity of an agonist as was previously suggested (Kaniaková et al., 2011), co-applications of a fixed concentration of (−)-lobeline and increasing concentrations of (±)-epibatidine were performed (Fig. 1B and D). The results confirm the antagonistic activity of (−)-lobeline at both AChR subtypes, and discard the possibility of potentiating activity.

3.2. Binding affinity of (−)-lobeline at the hα4β4 and hα4β2 AChRs

To compare the binding affinity of (−)-lobeline between the hα4β4 and hα4β2 AChRs, the effect of (−)-lobeline on [^{3}H]cytisine binding to either AChR was determined. The K_i values demonstrate that (−)-lobeline binds to the hα4β4 AChR (Fig. 2A) with ~3-fold higher affinity (1.82 ± 0.07 nM) compared to that for the hα4β2 AChR (Fig. 2B) (4.90 ± 0.30 nM) (Table 1). The fact that the calculated n_H values for the hα4β2 and hα4β4 AChRs are close to unity (Table 1) suggests that (−)-lobeline inhibits radioligand binding in a non-cooperative manner. This suggests, in turn, that (−)-lobeline and [^{3}H]cytisine bind to overlapping sites.

3.3. Molecular interactions of (−)-lobeline docked to either the α4β2 or α4β4 pocket

Molecular modeling and molecular dynamics were used to explain our experimental results. More specifically, to determine relevant differences between the hα4β2 and hα4β4 AChRs when (−)-lobeline interacts to each binding site domain, by comparing the molecular behavior of (−)-lobeline in its Apo and bound forms. Table 3 shows the hydrophobic and hydrogen bond interactions of (−)-lobeline with the respective α4β2 and α4β4 pockets. The opposite direction of Loop C when (−)-lobeline binds to the α4β2 or α4β4 pocket (Fig. 3) is reflected on the interactions shown in Table 3 since most of the initial contacts of the α4β2 principal component with (−)-lobeline are lost at the end of the simulation. From the thirteen interactions, eight are lost, five of which were originally shared with both AChBPs. As a consequence of this movement, α4β2 gains two interactions, one at position 8 (α4-Asp157, Loop B) and another at position 13 (α4-Ala199, Loop C). At the complementary component, α4β2 loses one original interaction (Val111 at position 21, Loop E), but acquires two, one at position 18 (Trp57, Loop D) and another at position 24 (Thr173, Loop F). In the α4β4 pocket, from the eleven interactions originally present at the principal component, only two were lost, α4-Cys198 (position12, Loop C) and α4-Asp204 (position 17, Loop C). At the same time, three newer interactions appeared, at positions 7 (α4-Tyr156, Loop B), 8 (α4-Asp157, Loop B; also newer in α4β2), and 14 (α4-Glu200, Loop C). At the complementary component, α4β4 lost two interactions, at positions 22 and 23 (β4-Leu121 and -Leu123, Loop E), but acquired one interaction at position 19 (β4-Ile81, Loop D). Overall, the number of residues from the α4β2 or α4β4 pocket interacting

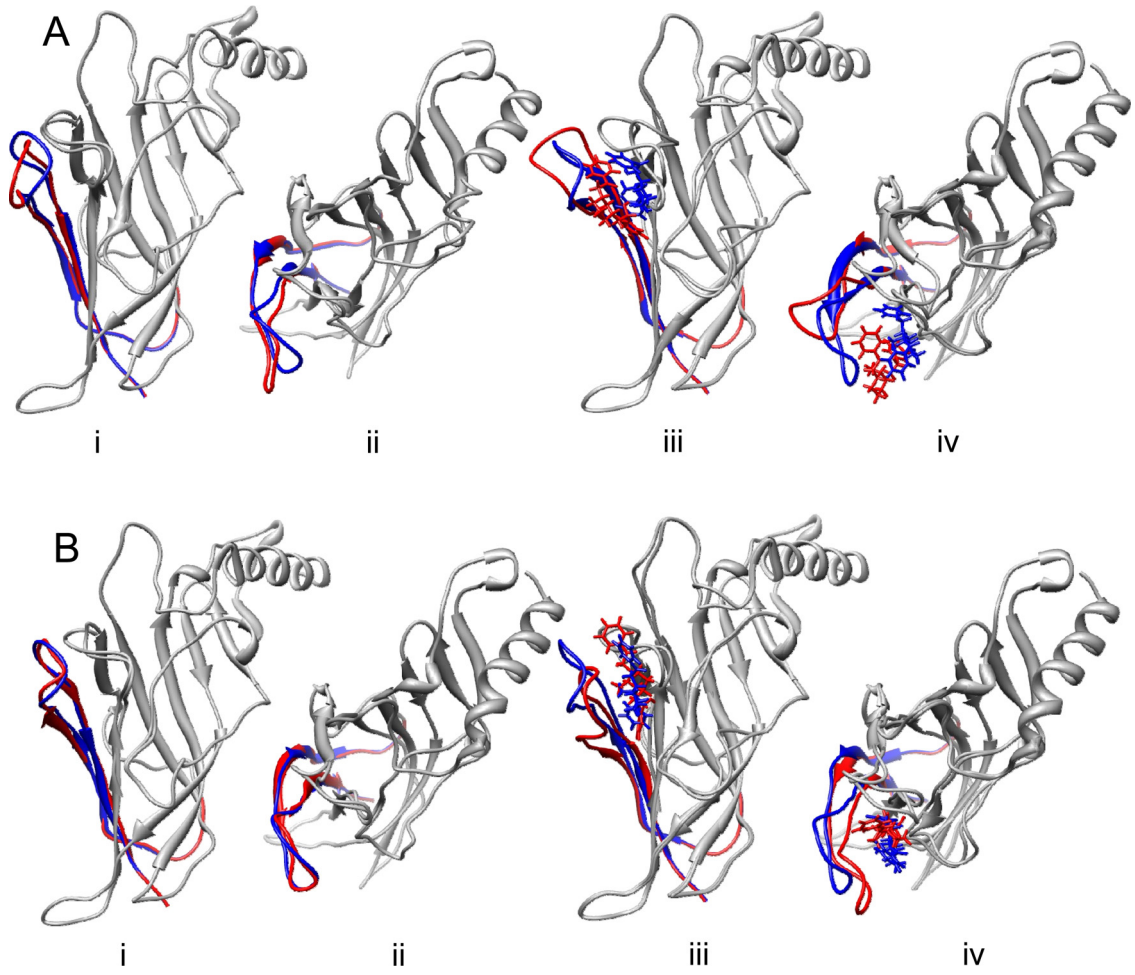

Fig. 3. Molecular dynamics (MD) simulations of the α4β2 (A) and α4β4 (B) subunit pairs, in the absence (i.e., Apo form; i, ii) and presence (i.e., bound form; iii, iv) of (−)-lobeline. Only the α4 (principal component) extracellular domains are shown for clarity (gray). The positions of Loop C and (−)-lobeline are shown at the beginning (blue) and at the end (red) of the 20-ns MD simulations. Simulations as seen from the hidden β-subunit (i and iii) and extracellular side (ii and iv), respectively. (For interpretation of the references to color in this figure legend, the reader is referred to the web version of this article.)

with (−)-lobeline at the end of the MD simulations is very similar, 12 and 14, respectively.

There are four positions in the aligned sequences that are consistently present in the binding of (−)-lobeline to their respective receptors, i.e. relative positions 1 (Loop A), 5 (Loop B), 10 (Loop C), and 15 (Loop C), all of which are aromatic residues at the principal component from the α4 subunit (Table 3) or AChBPs (Billen et al., 2012; Hansen et al., 2005), respectively. Moreover, (−)-lobeline makes contacts with these residues during the whole MD at both α4β2 and α4β4 pockets. These results support the view that these amino acids are structural components for the (−)-lobeline binding site.

Since the number of hydrophobic interactions for (−)-lobeline are very similar for both α4β2 and α4β4 pockets, the difference in the observed binding affinities (Table 1) probably comes from the hydrogen bonding pattern. The number of hydrogen bonds remains almost near zero for the α4β2 pocket during the whole simulation (measured every 100 fs), while in the α4β4 pocket, it increases sharply near the middle of the MD (Fig. 4A). In the α4β2 pocket, only residues from the principal component are involved. For example, the hydrogen bond with the highest occupancy (∼0.1%) is that with α4-Ser153 chain atoms, whereas other residues involved in hydrogen bonding have even less occupancy (Table 3). On the contrary, in the α4β4 pocket, a higher occupancy (∼18%) is observed for hydrogen bonds formed between the α4-Asp157 side chain and (−)-lobeline (Fig. 4B), followed by 0.64% occupancy at the α4-Gly152. Three more α4 residues are also involved in hydrogen bonding and one from the complementary component (Table 3).

3.4. Rotameric states of α4-Tyr98 at Loop A

The X-ray structures of (−)-lobeline complexed with different AChBPs (Billen et al., 2012; Hansen et al., 2005) showed that this drug exposes a subpocket in its binding domain by changing the rotameric state of a Tyr located in Loop A from the normal *g*− to the *t*− conformation, the so-called *g*-to-*t* or Tyr-flip conformation (reviewed in Arias, 2012). The homologous residue in the studied AChRs is α4-Tyr98 (position 1, Table 3) (Billen et al., 2012; Hansen et al., 2005). The analysis of the rotameric states in the α4β2 subpocket shows that α4-Tyr98 remains in the *t*− conformation approximately half of the simulation (54.67%), but then switches to the *g*− rotamer until the end of the MD (45.28%), and also remains for a short period in the *t*+ conformation (0.05%) (Fig. 5, Table 4). This causes that (−)-lobeline cannot longer remain in its subpocket. On the contrary, in the case of the α4β4 subpocket, α4-Tyr98 is mainly in the *t*− conformation (71.36%), but continuously and briefly alternates to the *t*+ rotamer (28.47%), and to *g*− (0.17%), allowing (−)-lobeline to remain in its subpocket, and thus, allowing the Loop C to approach and cap the binding pocket. Although in *t*+ the α4-Tyr98 side chain rotates 180° in opposite direction

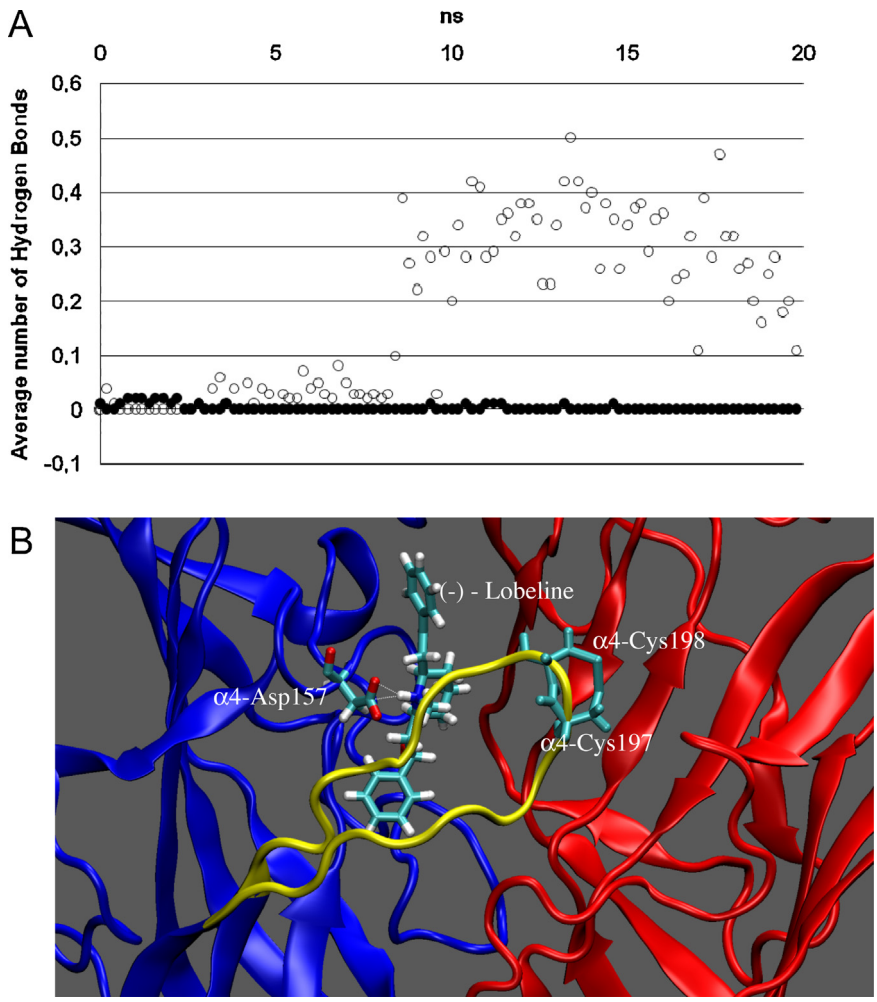

Fig. 4. (A) Average number of hydrogen bonds for the interaction of (−)-lobeline to each α4β2 (●) and α4β4 (○) subunit pair. The average number of hydrogen bonds was calculated as the mobile average in a temporal window of 100 fs during 20-ns MD simulations. (B) Detailed view of the hydrogen bonds (white dotted lines) formed between α4-Asp157 and the NH-hydrogen from (−)-lobeline (represented as sticks) in the α4β4 pocket. This hydrogen is present during 18% of the simulation time in the (−)-lobeline-α4β4 complex. Additional important residues are also depicted, including α4-Asp157, α4-Cys197, and α4-Cys198. The α4 (blue) and β4 (red) subunits are represented as ribbons. The Loop C (yellow) includes the Cys–Cys pair (gray). (For interpretation of the references to color in this figure legend, the reader is referred to the web version of this article.)

to *t*−, both rotamers are equivalent in maintaining the subpocket exposed, so the α-hydroxyphenetyl moiety of (−)-lobeline can occupy it.

3.5. *Molecular dynamics of (−)-lobeline docked to either the α4β2 or α4β4 pocket*

MD simulations (20-ns) were performed primarily to compare the behavior of Loop C in the absence (i.e., Apo form) and the presence of (−)-lobeline (i.e., bound form). Fig. 3 shows the behavior of Loop C from the α4β2 (Fig. 3A) and α4β4 (Fig. 3B) subunit pairs, without (Fig. 3Ai,ii and Bi,ii) and with (−)-lobeline (Fig. 3Aiii,iv and Biii,iv). In the Apo form, Loop C, after a short rearrangement, remains almost in the same position during the simulations (Fig. 3Ai,ii and Bi,ii). On the contrary, when (−)-lobeline is bound, the behavior of Loop C depends on the AChR site. In the α4β2 pocket, both Loop C and (−)-lobeline move opposite from the binding pocket situated at the subunit interface (Fig. 3Aiii,iv), while in the α4β4 pocket, although (−)-lobeline remains almost in its original position, Loop C moves toward the binding pocket promoting its closure.

Fig. 6 shows different views of these events in terms of the inter-molecular and translational conformational changes of Loop C (i.e., RMSD values) in the absence and the presence of (−)-lobeline as well as of the drug in its binding pocket. When the system is already stabilized (i.e., during the last 10-ns of simulation), the RMSD values for Loop C in the Apo form are 2.11 ± 0.01 (α4β2) and 1.83 ± 0.01 (α4β4), respectively (Fig. 6A), where the standard deviation (SD) values indicate that Loop C remains stable after an initial short movement. In the bound state, the RMSD values for Loop C are 2.25 ± 0.04 (α4β2) and 3.12 ± 0.01 (α4β4), respectively (Fig. 6B), suggesting that (−)-lobeline induces a slightly larger rearrangement of Loop C at the α4β4 pocket compared to that at the α4β2 pocket. However, these arrangements occur in opposite directions: in α4β2, away from the binding pocket, and in α4β4, toward it. The evidence that Loop C remains in its original position during the MDs of the Apo forms indicates that the observed opposite direction on Loop C is mediated by its interaction with (−)-lobeline and not by intrinsic features of these receptor subtypes. As indicated by the RMSD SD values during the second half of the simulation, the movement of Loop C in α4β4 is also less variable, suggesting that its interaction with (−)-lobeline is more stable. Although the RMSD values for (−)-lobeline are quite similar, 2.60 ± 0.27 (α4β2) and 2.77 ± 0.08 (α4β4), respectively (Fig. 6C), the SD values suggest that (−)-lobeline is more stable in the α4β4 pocket. The energy calculations confirm this statement (Table 2).

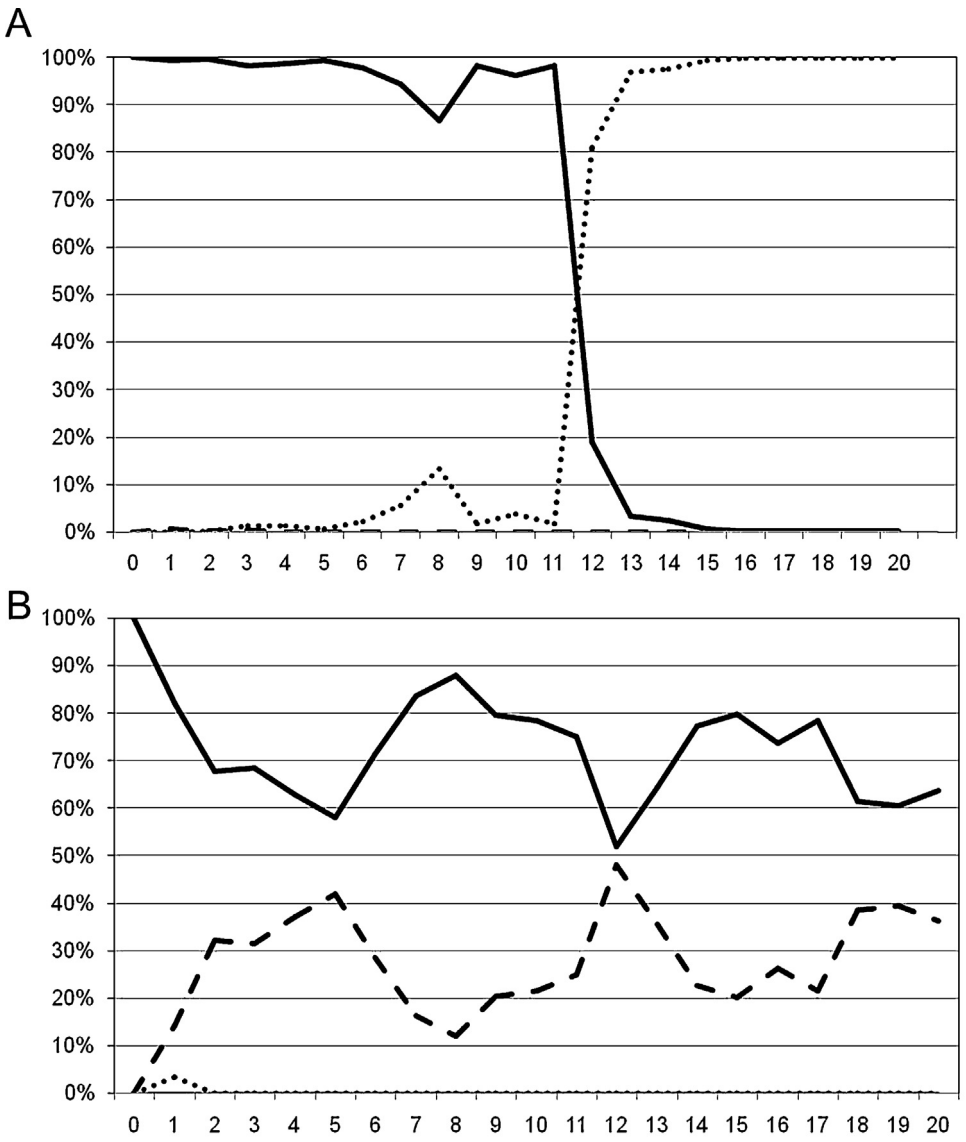

Fig. 5. Frequencies (percentages in the *Y*-axis) of the rotameric states of α4-Tyr98 observed during the 20-ns MD simulation when (−)-lobeline binds to the α4β2 (A) and α4β4 (B) subpockets, respectively. Observed frequencies (%) for the *t*− (—), *t*+ (−), and *g*− (. . .) rotameric states, respectively.

At the minimized state, the binding energy of (−)-lobeline for α4β4 (−4393 kJ/mol) is ~4-fold more favorable than that for α4β2 (−987 kJ/mol). The average energies during the last 10-ns simulations showed slightly increased values for α4β2 (−1230 kJ/mol) compared to that for α4β4 (−1824 kJ/mol).

4. Discussion

To determine the structural and functional differences between hα4β2 and hα4β4 AChRs, the pharmacologic and molecular interaction of (−)-lobeline to each AChR subtype was compared.

The results from functional studies assessed by Ca^{2+} influx assays indicate that (−)-lobeline does not activate the hα4β2 and hα4β4 AChR subtypes. These results support previous studies indicating that this ligand does not activate AChRs (Damaj et al., 1997), but disagree with its original classification as a partial agonist of AChRs. The Ca^{2+} influx results also indicate that (−)-lobeline does not potentiate the studied AChR subtypes. Differences in the used methods might account for the lack of potentiating effect. More specifically, Kaniaková et al. (2011) determined the potentiating effect of (−)-lobeline by measuring the peak response mediated by ACh using the patch clamp technique, whereas the increase in intracellular Ca^{2+} (peak to baseline difference) elicited by (±)-epibatidine is monitored in our Ca^{2+} influx assays. Since the fractional Ca^{2+} influx mediated by hα4β2 AChRs expressed in HEK293-hα4β2 cells amounts to only 2.5% (Fucile, 2004), the small potentiating effect reported for (−)-lobeline at the α4β2 AChR (Kaniaková et al., 2011) might not be detectable in a system where only Ca^{2+} influx is assessed. Another cause might be that (±)-epibatidine, instead of ACh, was used in our experiments, which coincides with the fact that the potentiating effect of (−)-lobeline on (±)-epibatidine-evoked responses was much less marked compared to that using ACh (Kaniaková et al., 2011). Furthermore, species differences my account for the observed discrepancies, since Kaniaková et al. (2011) used rat α4β2 AChRs whereas our experiments were performed by using hα4β2 AChRs. Another potential explanation is that additional allosteric sites for (−)-lobeline might exist as determined for varenicline (Arias et al., 2015) and cytisine (Arias et al., 2013), but did this possibility was not explored further.

The Ca^{2+} influx results also indicate that (−)-lobeline inhibits hα4β4 and hα4β2 AChRs by a competitive mechanism.

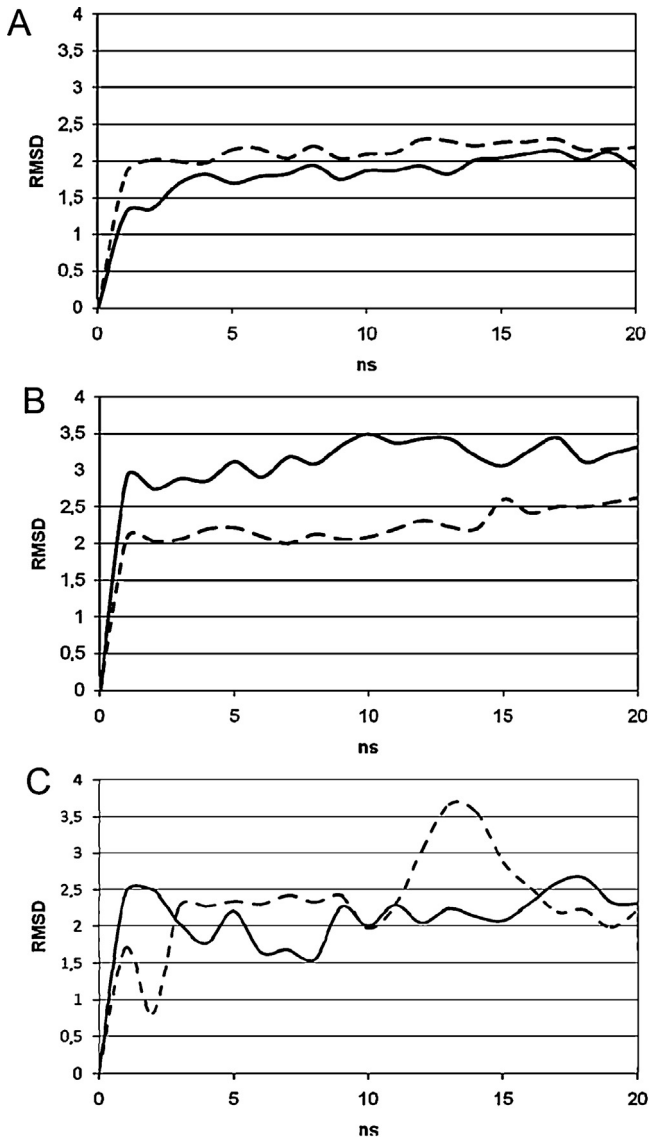

Fig. 6. RMSD values for Loop C in the absence (i.e., Apo form) (A) and the presence of (−)-lobeline (i.e., bound form) (B), and for (−)-lobeline bound at the respective subunit combinations (C). Braking and solid lines correspond to simulations at the α4β2 and α4β4 pockets, respectively.

Interestingly, (−)-lobeline inhibits the hα4β4 AChR with ~10-fold higher potency than that for the hα4β2 AChR (Table 1). In comparison, (±)-epibatidine has ~3-fold higher potency for hα4β4 AChRs compared to that for hα4β2 AChRs. The simplest explanation for the different potency is that (−)-lobeline binds the hα4β4 AChR agonist sites with higher affinity than that for the hα4β2 AChR, as demonstrated by our [^{3}H]cytisine competition binding results (Table 1). Another difference is that although (−)-lobeline inhibits [^{3}H]cytisine binding to each AChR by a non-cooperative mechanism, it inhibits (±)-epibatidine-evoked hα4β4 AChR activity by a cooperative mechanism, opposite to the non-cooperative mechanism observed for the hα4β2 AChR. These results suggest that the (−)-lobeline inhibitory mechanism at the hα4β4 AChR is more complex than that at the hα4β2 AChR. A possibility is that in addition to a competitive mechanism of inhibition, (−)-lobeline might induce, for example, receptor desensitization or even ion channel blockade at higher proportions than that at the hα4β2 AChR.

A dose of 1 mg/kg (−)-lobeline, which produces anti-addictive activity (e.g., see Polston et al., 2006), can reach the plasma at a maximal concentration of ~1.4 μM (Lin et al., 2013). Considering that (−)-lobeline can cross the blood-brain-barrier, it is clear that (−)-lobeline can inhibit these AChR subtypes at significant doses. These results corroborate previous studies and support the possibility that hα4β4 AChRs are also targets for the pharmacological and clinical activity of (−)-lobeline. In this regard, α4β4 AChRs are expressed in several brain regions implicated in drug addiction, including basal ganglia, midbrain, ventral tegmental area, hippocampus, and cortex (Azam et al., 2002; Quik et al., 2000).

The molecular interactions of (−)-lobeline with residues from the α4β2 and α4β4 binding sites are complex (Table 3). At the initial and minimized state of the MDs, (−)-lobeline interacts with the principal and complementary components at each α4β2 and α4β4 interface, supporting previous results on the Ct-AChBP (Billen et al., 2012). For instance, the aromatic residues at positions 5 (Trp, Loop B), 10 (Tyr, Loop C), and 15 (Tyr, Loop C) are present in all AChRs and therefore, we conclude they are essential for (−)-lobeline binding. Although the Cys^{197}–Cys^{198} pair, present in Loop C from the hα4β2 AChR, makes contact with (−)-lobeline, these interactions are lost at the end of the simulation when the Loop C moves away from the drug (and the binding pocket). On the other hand, α4-Cys^{197}, at position 11, from the hα4β4, does not make a close contact with (−)-lobeline.

More importantly for the comprehension of the experimental data is that the MDs studies give a structural explanation for the different (−)-lobeline affinity at each AChR subtype. The observed higher affinity is based on at least four structural and dynamics features: (1) higher stability of the hydrogen bonds for (−)-lobeline at the α4β4 pocket that is lacking in the α4β2 pocket (Table 3, Fig. 4); (2) higher stability of (−)-lobeline within the α4β4 pocket during the last 10-ns MD simulations compared to that at the α4β2 pocket (Fig. 6C); (3) higher stability of Loop C when (−)-lobeline binds to α4β4 compared to that for α4β2. More specifically, (−)-lobeline promotes Loop C to cap the binding site at the α4β4 interface, as observed in the high resolution images of this ligand bound to AChBPs (Billen et al., 2012; Hansen et al., 2005; reviewed in Arias, 2012), while (−)-lobeline forces Loop C to get apart from the α4β2 binding site; and (4) the orientation of (−)-lobeline within the α4β4 subpocket, but not in the α4β2 subpocket, promoted by the *t*− (or *t*+) rotameric state of α4-Tyr98, remains unchanged during the whole MD simulation, allowing the formation of stable hydrogen

Table 2
Potential energy values for the α4β2 and α4β4 pockets, in the absence (Apo state) and in the presence of (−)-lobeline, and emulated binding energies for (−)-lobeline.

	Energy (kJ/mol)					Emulated binding energy (kJ/mol)	
	α4β2 pocket		α4β4 pocket		(−)-Lobeline	α4β2	α4β4
	Apo	Bound (−)-lobeline	Apo	Bound (−)-lobeline			
MD initial state	−14,108	−14,937	−11,929	−16,163	159	−987	−4393
Mean MD (last 10 ns)	−7552	−8623	−7117	−8782	159	−1230	−1824

Potential energies at the initial state of MDs are those calculated after minimizing the molecular systems as described in Section 2. Mean energies are the energy averages estimated during the last 10,000 steps (1 step, 1 fs) of MD.

Table 3
Molecular interactions of (−)-lobeline with the agonist binding sites at the α4β2 and α4β4 interfaces.

Position #	α4β2 pocket				α4β4 pocket				Loop	Secondary structure
	Principal component									
	Residue	I	F	Hydrogen bond	Residue	I	F	Hydrogen bond		
1	Y98	√	√			√	√		A	Loop
2	F151	√				√	√		B	β-Strand 7
3	G152	√				√	√	0.64 M	B	β-Strand 7
4	S153	√		0.10M		√	√	0.03 M	B	β-Strand 7
5	W154	√	√	0.03 M		√	√	0.00 S	B	Loop
6	T155	√	√	0.01 S		√	√		B	Loop
7	Y156						√	0.00 M	B	Loop
8	D157		√				√	18.10 S	B	Loop
9	R193	√	√						C	β-Strand 9
10	Y195	√	√			√	√		C	β-Strand 9
11	C197	√							C	Loop
12	C198	√				√			C	Loop
13	A199		√						C	Loop
14	E200						√		C	Loop
15	Y202	√	√	0.05 S		√	√		C	Loop
16	P203	√				√	√		C	β-Strand 10
17	D204	√				√			C	β-Strand 10

Position #	α4β2 pocket				α4β4 pocket				Loop	Secondary structure
	Complementary component									
	Residue	I	F	Hydrogen bond	Residue	I	F	Hydrogen bond		
18	W57		√		W59			D	β-Strand 2	
19	K79				I81	√		D	β-Strand 3	
20	N109				N111		0.01 S	E	β-Strand 5	
21	V111	√			I113	√	√		E	β-Strand 5
22	F119	√	√		L121	√			E	β-Strand 6
23	L121	√	√		L123	√			E	Loop
24	T173		√		T175			F	Loop	

I and F: respective initial and final step of the MD; √: present interaction.
In "Hydrogen bonds", the numbers indicate occupancy, i.e., the percentage that the hydrogen bond is maintained during the simulation time; M: indicates the amino acid backbone atoms involved in the hydrogen bonding; and S: side chain atoms involved in hydrogen bonding.

Table 4
Rotameric states of α4-Tyr98 from Loop A during the MD simulations of (−)-lobeline bound to the α4β2 or α4β4 subpocket.

AChR subunit pair	*t*−	*t*+	*g*+	*g*−
α4β2	54.67%	0.05%	0.0%	45.28%
α4β4	71.36%	28.47%	0.0%	0.17%

The duration of a particular rotameric state (*t*− and *t*+ rotate 180° in opposite direction, whereas *g*+ and *g*− rotate 60° in opposite direction) of α4-Tyr98 during the 20-ns MD simulation is represented as percentages. No SD values were included since there is only one simulation for each subunit pair.

bonds and capping of Loop C in the binding site. This key residue, located at position 1, is present in all AChRs except in Ct-AChBP in which a Phe is found.

This work gives a detailed view of the molecular and dynamics events evoked by (−)-lobeline supporting the differential binding affinity and subsequent inhibitory potency between hα4β2 and hα4β4 AChRs.

Acknowledgement

This research was supported by a grant from the Consejo Nacional de Investigaciones Científicas y Técnicas (CONICET; Argentina) (to M.O.O.).

References

Arias HR. Allosteric modulation of nicotine acetylcholine receptors. In: Arias HR, editor. Pharmacology of Nicotinic Acetylcholine Receptors from the Basic and Therapeutic Perspectives. Kerala, India: Research Signpost; 2011. p. 151–73.

Arias HR. Molecular interactions between ligands and nicotinic acetylcholine receptors revealed by studies with acetylcholine binding proteins. J Thermodynam Catal 2012;3:116.

Arias HR, Targowska-Duda KM, Feuerbach D, Jozwiak K. Mecamylamine inhibits muscle nicotinic acetylcholine receptors by competitive and noncompetitive mechanisms. OA Biochemistry 2013;1:7.

Arias HR, Feuerbach D, Targowska-Duda KM, Kaczor AA, Poso A, Jozwiak K. Pharmacological and molecular studies on the interaction of varenicline with different nicotinic acetylcholine receptor subtypes. Potential mechanism underlying partial agonism at human α4β2 and α3β4 subtypes. Biochem Biophys Acta Biomembr 2015;1848:731–41.

Azam L, Winzer-Serhan UH, Chen Y, Leslie FM. Expression of neuronal nicotinic acetylcholine receptor subunit mRNAs within midbrain dopamine neurons. J Comp Neurol 2002;444:260–74.

Billen B, Spurny R, Brams M, Van Elk R, Valera-Kummer S, Yakel JL, et al. Molecular actions of smoking cessation drugs at α4β2 nicotinic receptors defined in crystal structures of a homologous binding protein. Proc Natl Acad Sci U S A 2012;109:9173–8.

Brioni JD, O'Neill AB, Kim DJ, Decker MW. Nicotinic receptor agonists exhibit anxiolytic-like effects on the elevated plus-maze test. Eur J Pharmacol 1993;238:1–8.

Brooks BR, Bruccoleri RE, Olafson BD, States DJ, Swaminathan S, Karplus M. CHARMM: a program for macromolecular energy, minimization, and dynamics calculations. J Comput Chem 1983;4:187–217.

Cheng Y, Prusoff WH. Relationship between the inhibition constant (K_i) and the concentration of inhibitor which causes 50 percent inhibition (IC_{50}) of an enzymatic reaction. Biochem Pharmacol 1973;22:3099–108.

Damaj MI, Patrick GS, Creasy KR, Martin BR. Pharmacology of lobeline, a nicotinic receptor ligand. J Pharmacol Exp Ther 1997;282:410–9.

Decker MW, Majchrzak MJ, Arnerić SP. Effects of lobeline, a nicotinic receptor agonist, on learning and memory. Pharmacol Biochem Behav 1993;45:571–6.

Dwoskin LP, Crooks PA. A novel mechanism of action and potential use for lobeline as a treatment for psychostimulant abuse. Biochem Pharmacol 2002;63:89–98.

Flammia D, Dukat M, Damaj MI, Martin B, Glennon RA. Lobeline: structure–affinity investigation of nicotinic acetylcholinergic receptor binding. J Med Chem 1999;42:3726–31.

Fucile S. Ca^{2+} permeability of nicotinic acetylcholine receptors. Cell Calcium 2004;35:1–8.

Grady SR, Meinerz NM, Cao J, Reynolds AM, Picciotto MR, Changeux J-P, et al. Nicotinic agonists stimulate acetylcholine release from mouse interpeduncular

nucleus: a function mediated by a different nAChR than dopamine release from striatum. J Neurochem 2001;76:258–68.
Hansen S, Sulzenbacher G, Huxford T, Marchot P, Taylor P, Bourne Y. Structures of *Aplysia* AChBP complexes with nicotinic agonists and antagonists reveal distinctive binding interfaces and conformations. EMBO J 2005;24:2625–46.
Harrod SB, Dwoskin LP, Crooks PA, Klebaur JE, Bardo MT. Lobeline attenuates D-methamphetamine self-administration in rats. J Pharmacol Exp Ther 2001;298:172–9.
Humphrey W, Dalke A, Schulten K. VMD – visual molecular dynamics. J Mol Graphics 1996;14:33–8.
Kaniaková M, Lindovský J, Krůšek J, Adámek S, Vyskočil F. Dual effect of lobeline on α4β2 rat neuronal nicotinic receptors. Eur J Pharmacol 2011;658:108–13.
Keserü G, Kolossváry I. Molecular mechanics and conformational analysis in drug design. Oxford, UK: Blackwell Science Ltd; 1999.
Lewards EG. Computational chemistry. Introduction to the theory and applications of molecular and quantum mechanics. 2nd ed. New York: Springer; 2011.
Lin C, Han F, Guo Z, Lin G. Pharmacokinetic study of lobeline in rats after intravenous and oral administration. Lat Am J Pharm 2013;32:1575–7.
Martin CA, Nuzzo PA, Ranseen JD, Kleven MS, Guenthner G, Williams Y, et al. Lobeline effects on cognitive performance in adult ADHD. J Atten Disord 2015 [PMID: 23966351].
Mathur A, Shankaracharya Vidyarthi AS. SWIFT MODELLER: a JAVA based GUI for molecular modeling. J Mol Model 2011;17:2601–7.
Ortells MO, Arias HR. Neuronal networks of nicotine addiction. Int J Biochem Cell Biol 2010;42:1931–5.
Pedretti A, Villa L, Vistoli G. VEGA – an open platform to develop chemo-bioinformatics applications, using plug-in architecture and script programming. J Comput Aided Mol Des 2004;18:167–73.
Pérez EG, Ocampo C, Feuerbach D, López JJ, Morelo GL, Tapia RA, et al. Novel 1-(1-benzyl-1*H*-indol-3-yl)-*N*,*N*,*N*-trimethylmethanaminium iodides are competitive antagonists of the human α4β2 and α7 nicotinic acetylcholine receptors. Med Chem Commun 2013;4:1166–70.
Phillips JC, Braun R, Wang W, Gumbart J, Tajkhorshid E, Villa E, et al. Scalable molecular dynamics with NAMD. J Comput Chem 2005;26:1781–802.
Picciotto MR, Zoli M, Rimondini R, Lena C, Marubio LM, Pich EM, et al. Acetylcholine receptors containing the β2 subunit are involved in the reinforcing properties of nicotine. Nature 1998;391:173–7.
Polston JE, Cunningham CS, Rodvelt KR, Miller DK. Lobeline augments and inhibits cocaine-induced hyperactivity in rats. Life Sci 2006;79:981–90.
Quik M, Polonskaya Y, Gillespie A, Jakowec M, Lloyd GK, Langston JW. Localization of nicotinic receptor subunit mRNAs in monkey brain by *in situ* hybridization. J Comp Neurol 2000;425:58–69.
Šali A, Blundell TL. Comparative protein modelling by satisfaction of spatial restraints. J Mol Biol 1993;234:779–815.
Sewester CS, Threlkeld DS, Olin BR, Heirendt P, Simo RA, Hinton TL, et al. Smoking deterrents. In: Sewester CS, Threlkeld DS, Olin BR, Heirendt P, Simo RA, Hinton TL, Hebel SK, Hagemann RC, Rivard R, editors. Drug facts and comparisons. St. Louis: Lippincott; 1997. p. 3470.
Shoaib M, Gommans J, Morley A, Stolerman IP, Grailhe R, Changeux J. The role of nicotinic receptor beta-2 subunits in nicotine discrimination and conditioned taste aversion. Neuropharmacology 2002;42:530–9.
Slater YE, Houlihan LM, Maskell PD, Exley R, Bermudez I, Lukas RJ, et al. Halogenated cytisine derivatives as agonists at human neuronal nicotinic acetylcholine receptor subtypes. Neuropharmacology 2003;44:503–15.
Stauderman KA, Mahaffy LS, Akong M, Veliçelebi G, Chavez-Noriega LE, Crona JH, et al. Characterization of human recombinant neuronal nicotinic acetylcholine receptor subunit combinations α2β4, α3β4 and α4β4 stably expressed in HEK293 cells. J Pharmacol Exp Ther 1998;284:777–89.
Thompson JD, Higgins DG, Gibson TJ. CLUSTAL W: improving the sensitivity of progressive multiple sequence Alignment through sequence weighting, position-specific gap penalties and weight matrix choice. Nucleic Acids Res 1994;22:4673–80.
Zhang J, Steinbach JH. Cytisine binds with similar affinity to nicotinic α4β2 receptors on the cell surface and in homogenates. Brain Res 2003;959:98–102.